Heliyon 8 (2023) e12630

Contents lists available at ScienceDirect

Heliyon

journal homepage: www.cell.com/heliyon

Research article

One-step generation of a conditional allele in mice using a short artificial intron

Annelise M. Cassidy [a], Destinée B. Thomas [a], Emin Kuliyev [b], Hanying Chen [a], Stephane Pelletier [a,*]

[a] Department of Medical and Molecular Genetics, Indiana University School of Medicine, Indiana University—Purdue University Indianapolis, Indianapolis, IN, 46202, USA
[b] Department of Immunology, St. Jude Children's Research Hospital, Memphis, TN, 38105, USA

ARTICLE INFO

Keywords:
Conditional allele
Artificial intron
Mouse model
CRISPR-Cas9
Scyl1

ABSTRACT

Despite tremendous advances in genome editing technologies, generation of conditional alleles in mice has remained challenging. Recent studies in cells have successfully made use of short artificial introns to engineer conditional alleles. The approach consists of inserting a small cassette within an exon of a gene using CRISPR-Cas9 technology. The cassette, referred to as Artificial Intron version 4 (AIv4), contains sequences encoding a splice donor, essential intronic sequences flanked by loxP sites and a splice acceptor site. Under normal conditions, the artificial intron is removed by the splicing machinery, allowing for proper expression of the gene product. Following Cre-mediated recombination of the two loxP sites, the intron is disabled, and splicing can no longer occur. The remaining intronic sequences create a frameshift and early translation termination. Here we describe the application of this technology to engineer a conditional allele in mice using *Scyl1* as a model gene. Insertion of the cassette occurred in 17% of edited mice obtained from pronuclear stage zygote microinjection. Mice homozygous for the insertion expressed SCYL1 at levels comparable to wild-type mice and showed no overt abnormalities associated with the loss of *Scyl1* function, indicating the proper removal of the artificial intron. Inactivation of the cassette via Cre-mediated recombination in vivo occurred at high frequency, abrogated SCYL1 protein expression, and resulted in loss-of-function phenotypes. Our results broaden the applicability of this approach to engineering conditional alleles in mice.

1. Introduction

Genetically modified mouse models have been instrumental in understanding gene function and modeling human disease. The engineering of mouse models has been greatly simplified with the discovery and implementation of targetable nucleases such as Clustered Regularly Interspaced Short Palindromic Repeats (CRISPR)-CRISPR-associated protein 9 (Cas9) systems for genome editing. These enzymes function by introducing DNA double strand breaks (DSBs) at a precise location within a genome of interest which in turn activate DNA repair pathways that can be overtaken to introduce specific mutations by the coadministration of DNA repair templates (Pelletier et al., 2015).

Despite these technological advances, the generation of mouse models with conditional alleles has remained challenging. Two main strategies are currently used to engineer these models. The first strategy consists of flanking one or more critical exons of a gene with site specific recombinase sequences (SSRSs) such that upon recombination between the two SSRSs, the intervening region is eliminated. Alleles are typically designed such that splicing between the remaining exons results in a frame shift and the generation of a premature stop codons, leading to early termination of translation and, depending on the location of the newly generated stop codon(s) within the gene, degradation of the defective mRNA transcript via the nonsense-mediated mRNA decay pathway (Popp and Maquat, 2016). The second strategy involves the insertion of large and complex artificial introns within an exon of a gene. Two artificial intron designs have been described, the conditional by inversion (COIN) and CRISPR-FLIP (Andersson-Rolf et al., 2017; Economides et al., 2013). The COIN design makes use an optimized conditional gene trap module (COIN module) that lies antisense of the target gene. Upon Cre exposure, the COIN module is inverted, resulting in the expression of a reporter gene and termination of translation of the target gene. Similarly, CRISPR-FLIP makes use of an inverted puromycin STOP cassette module that lies inert, antisense of the

* Corresponding author.
E-mail address: spellet@iu.edu (S. Pelletier).

https://doi.org/10.1016/j.heliyon.2022.e12630
Received 25 August 2022; Received in revised form 20 October 2022; Accepted 19 December 2022

target gene. Upon Cre exposure, the cassette is inverted, resulting in the inactivation of the allele. Both strategies can be used for engineering mouse models via conventional or CRISPR-assisted gene targeting in embryonic stem (ES) cells. While these approaches have been used to engineer countless mouse models with conditional alleles, they are inefficient, labor intensive, and very expensive. Moreover, the presence of strong promoters within reporter cassettes may have an impact on expression of surrounding genes (Soulez et al., 2019).

A simpler version of the artificial intron approach called DEgradation based on Cre-regulated-Artificial Intron (DECAI) was recently described in cultured cells (Guzzardo et al., 2017). In this system, a short DNA cassette containing a splice donor site, essential intronic sequences flanked by two loxP sites and a splice acceptor site is inserted within an exon of a target gene. In the absence of Cre, the artificial intron is recognized and removed by the splicing machinery allowing for normal expression of the protein. In the presence of Cre, the intron is inactivated and sequences, including a string of stop codons in all three frames, remain within the transcript, resulting in early translation termination and degradation of the faulty mRNA transcript through the nonsense-mediated mRNA decay pathway. While the approach was successful in cultured cells, it has never been used to engineer mouse models. Implementing this strategy may have a significant impact on

Table 1

1Reagent	Source	Catalog #	Unique Identifier or Sequence
B6.C-Tg (CMV-cre)1Cgn/J mouse model	The Jackson Laboratory	006054	
Scyl1^{FL} mouse model	Pelletier Lab		*Name of the allele:* SCY1-like 1 (S. cerevisiae); targeted mutation 1.1, Stephane Pelletier
			Allele symbol: Scyl1$^{tm1.1Spel}$
Scyl1^{AIv4} mouse model	Pelletier Lab		*Name of the allele:* SCY1-like 1 (S. cerevisiae); targeted mutation 2, Stephane Pelletier
			Allele symbol: Scyl1^{tm2Spel}
Scyl1- mouse model	Pelletier Lab		*Name of the allele:* SCY1-like 1 (S. cerevisiae); targeted mutation 1, Stephane Pelletier
			Allele symbol: Scyl1^{tm1Spel}
S1E154D-F1	Integrated DNA Technologies		TACTCTCCTCAGGCCCTCAC
S1E154D-R1	Integrated DNA Technologies		GAAGCACCGAACACCCAAAC
Cre66	Integrated DNA Technologies		CCTGCGGTGCTAACCAGCGTT
Cre99	Integrated DNA Technologies		TGGGCGGCATGGTGCAAGTT
S1F01	Integrated DNA Technologies		GCTGCTCCGAAGGCCGCGGCCGA
S1R02	Integrated DNA Technologies		GAGGAGAGTAAGATGGGTAGA
S1R51	Integrated DNA Technologies		GATTATGTACACTAGATGTGCCTGA
Scyl1_AIv4_F51	Integrated DNA Technologies		GTGCCTCCACATCGTGACAG
Scyl1_AIv4_R52	Integrated DNA Technologies		CTCCGGGGGATCATACTGCT
Scyl1_AIv4_HDR	Integrated DNA Technologies		AGATCGTGAAAGCCCTCAGCTTCCTGGTCAACGACTGCA ACCTCATCCACAATAATGTGTAAGTAATAACTTCGTATA GCATACATTATACGAAGTTATTCAAGGTTAGAAGACAGG TTTAAGGAGACCAATGGAAACTGGGCTTGTCGAGACAGA GAAGACTCTTGCGTTTCTGATAGGCACCTATTGGTCTTAC TGACATCCACTTTGCCATAACTTCGTATAGCATACATTAT ACGAAGTTATTTTCTCTCCACAGCTGCATGGCCGCTGTGTT TGTGGACAGGGCTGGCGAGTGGAAACTTGGGGGTCT GGACTA
S1-HAN-Guide_01-F	Integrated DNA Technologies		TAATACGACTCACTATAGGCATCCA CAATAATGTCTGCAGTTTTAGAGCT AGAAATAGCA
RT-Scyl1_F21	Integrated DNA Technologies		CGCAGTGTCCATCTTCGTGTA
RT-Scyl1_R51	Integrated DNA Technologies		CCCGGCAGTTCTGCAGGAA
PhosSTOP™ Phosphatase Inhibitor Cocktail tablets	Sigma-Aldrich	4906837001	
cOmplete™, EDTA-free Protease Inhibitor Cocktail tablets	Sigma-Aldrich	4693132001	
Peirce BCA Assay	Life Technologies	23225	
10% Criterion™ XT Bis-Tris Protein Gels	Bio-Rad Laboratories	3450112	
Rneasy Maxi Kit	Qiagen	75162	
RNase-Free DNase Set	Qiagen	79254	
Taq DNA Polymerase	Qiagen	201205	
ProtoScript® II First Strand cDNA Synthesis Kit	New England Biolabs	E6560L	
OneTaq One-Step RT-PCR Kit	New England Biolabs	E5315S	
TaqMan Gene Expression Assay Probe – *Scyl1*	Applied Biosystems		Mm00452459_m1(FAM)
TaqMan Gene Expression Assay Probe – *Gapdh*	Applied Biosystems		Mm99999915_g1 (FAM)
TaqMan 2X Master Mix	Applied Biosystems	4444557	
Anti-SCYL1	Pelletier Lab	7645-AP	
Anti-SCYL1	Pelletier Lab	7691-AP	
Anti-β-actin	Sigma-Aldrich	A5441	AB_476744
Anti-HA-Tag Antibody (F-7)	Santa Cruz Biotechnology	sc-7392	
Peroxidase AffiniPure Donkey Anti-Rabbit IgG (H + L)	Jackson ImmunoResearch Lab	711-035-152	
StarBright Blue 700 Goat Anti-Mouse IgG	Bio-Rad	12004158	

improving the success rate, speed, and cost of generating conditional alleles in mice. Insertion of a short DNA segment as opposed to insertion of a large DNA constructs, or a pair of loxP sites flanked by homology arms, may reduce the number of microinjection sessions currently required for the generation of these mouse models. Short DNA constructs are also more affordable to produce and their insertion within the genome is easier to characterize.

Here we show the successful application of this approach for engineering conditional alleles in mice. The insertion of the short cassette within exon 3 of the Scyl1 gene occurred in 16.7% of edited mice obtained from microinjections. Mice homozygous for the insertion expressed SCYL1 to levels that are comparable to wild-type animals, illustrating the functionality of the allele. Incapacitation of the artificial intron by crossing these mice to Cre-deleter mice resulted in the complete inactivation of the allele and induced phenotypic changes consistent with the loss of *Scyl1* function. Mechanistically, we found that gene inactivation occurs not only at the transcriptional and translational levels, but also post-translationally.

2. Methods

2.1. Generation of $Scyl1^{AIv4}$ mice

$Scyl1^{AIv4}$ mice were engineered using CRISPR-Cas9 technology. Briefly, C57BL/6J zygotes were injected with Cas9 mRNA transcript (100 ng/μL), a sgRNA targeting exon 3 of *Scyl1* (50 ng/μL), and an HDR template in the form of a ssDNA molecule (1.2 pmol/μL, see Table 1 for complete sequences). Zygotes were then transferred to pseudopregnant CD1 females. Pups obtained from these microinjections were characterized by PCR-based genotyping and Sanger sequencing using the following primers: S1E154D-F1 5′-TACTCTCCTCAGGCCCTCAC-3′ and S1E154D-R1 5′-GAAGCACCGAACACCCAAAC-3'. A fragment of 667 bp was obtained for the wild-type allele, while the AIv4 allele produced a fragment of 868 bp. Sanger sequencing was performed using both forward and reverse primers. Guide sequence selection, HDR template design, and synthesis of Cas9 mRNA and sgRNA transcripts were performed as previously described in (Cassidy et al., 2022). The following primer was used for synthesis of the sgRNA: S1-HAN-Guide_01-F.

5′-TAATACGACTCACTATAGGCATCCACAA-TAATGTCTGCAGTTTTAGAGCTAGAAATAGCA-3'.

2.2. Sanger sequencing

Sanger sequencing was performed as previously described in (Cassidy et al., 2022).

2.3. Previously described mouse models used in this study

B6.C-Tg (CMV-cre)1Cgn/J, 006054 mice (CMV-Cre+) were purchased from Jackson Laboratory (Bar Harbor, ME). $Scyl1^{FL}$ mice ($Scyl1^{Tm1.1Spel}$) and $Scyl1^{-}$ ($Scyl1^{Tm1Spel}$) were generated in our laboratory and previously described in (Pelletier et al., 2012).

2.4. Generation of CMV-Cre+; $Scyl1^{AIv4\Delta}$ mice

CMV-Cre+;$Scyl1^{AIv4\Delta/AIv4\Delta}$ mice were generated first by crossing $Scyl1^{AIv4/AIv4}$ females with CMV-Cre + males (B6.C-Tg (CMV-cre)1Cgn/J, 006054). From this cross, we obtained CMV-Cre+;$Scyl1^{+/AIv4\Delta}$ females, which were then bred with $Scyl1^{AIv4/AIv4}$ males.

2.5. PCR genotyping

CMV-Cre + mice were routinely genotyped using the following primers: Cre66 5′-CCTGCGGTGCTAACCAGCGTT-3′ and Cre99 5′-TGGGCGGCATGGTGCAAGTT-3'. Mice positive for Cre recombinase produced a fragment of 470 bp, whereas no fragments were obtained from wild-type mice. Mice bearing $Scyl1^{AIv4}$ and $Scyl1^{AIv4\Delta}$ alleles were routinely genotyped using the following primers: Scyl1_AIv4_F51 5′-GTGCCTCCACATCGTGACAG-3′ and Scyl1_AIv4_R52 5′-CTCCGGGGGA TCATACTGCT-3'. These primers were designed to facilitate the distinction between the wild-type and the $Scyl1^{AIv4\Delta}$ alleles. Fragments of 505, 358, and 304 bp corresponding to the $Scyl1^{AIv4}$, $Scyl1^{AIv4\Delta}$, and wild-type alleles were obtained. Mice bearing the $Scyl1^{FL}$ and $Scyl1^{-}$ were routinely genotyped using the following primers: S1F01 (5′-GCTGCTCCGAA GGCCGCGGCCGA-3′), S1R51 (5′-GATTATGTACACTAGATGTGCCTGA-3′), and S1R02 (5′-GAGGAGAGTAAGATGGGTAGA-3′). Bands of 521, 251, and 625 bp corresponding to the wild-type ($Scyl1^{+}$), null ($Scyl1^{-}$), and floxed alleles ($Scyl1^{FL}$), respectively, were obtained. All PCR genotyping reactions were performed using Taq DNA polymerase from Qiagen (201205). Cre-mediated recombination of the AIv4 and floxed alleles was quantified by measuring the specific mean grey value of the band corresponding to the recombined allele divided by the sum of specific mean grey values of both the recombined and non-recombined alleles using NIH Image J software version 1.42q (http://rsbweb.nih.gov/ij). These values were multiplied by 100 to obtained percentages.

2.6. SCYL1 protein expression in mouse tissues

SCYL1 expression in the brains of $Scyl1^{+/+}$, $Scyl1^{+/-}$, $Scyl1^{-/-}$, $Scyl1^{AIv4/AIv4}$, CMV-Cre+;$Scyl1^{AIv4\Delta/AIv4\Delta}$, and CMV-Cre+;$Scyl1^{+/AIv4\Delta}$ was analyzed by Western blot. Briefly, brains were harvested, rinsed with PBS and snap frozen on dry ice. The brains were then lysed in Triton X-100 (Sigma-Aldrich, T8787-250ML) buffer [50 mM Tris-HCl, pH 8.0, 150 mM NaCl, 1% TX-100, PhosSTOP™ Phosphatase Inhibitor Cocktail tablets (4906837001, Sigma-Aldrich) and cOmplete™, EDTA-free Protease Inhibitor Cocktail tablets (4693132001, Sigma-Aldrich)]. Samples were cleared by centrifugation at 4 °C for 30 min, 5,000 x g and proteins were quantified using the Peirce BCA Assay (23225, Life Technologies). 5 μg of total protein were loaded on 10% Criterion™ XT Bis-Tris Protein Gels for separation. The resolved proteins were then transferred to LF-PVDF membranes and probed with an anti-SCYL1 antibody or b-actin antibody overnight at 4 °C in TBST (137 mM sodium chloride, 20 mM Tris, 0.1% Tween 20, pH 7.6) supplemented with 3% nonfat dry milk. The next day, the membranes were washed three times and probed with secondary antibodies for 1 h at room temperature. Following incubation with the secondary antibodies, the membranes were washed three times and the proteins detected by chemiluminescence or fluorescence using the ChemiDoc™ MP Imaging System. SCYL1 expression was quantified by using NIH Image J software version 1.42q (http://rsbweb.nih.gov/ij). For quantification, the specific mean grey values (excluding the mean grey value of the background) corresponding to the SCYL1 bands were divided by the specific mean grey value of the bands corresponding to β-actin.

2.7. Animal phenotyping

Phenotypic abnormalities in $Scyl1^{+/+}$, $Scyl1^{AIv4/AIv4}$, $Scyl1^{-/-}$, CMV-Cre+;$Scyl1^{AIv4\Delta/AIv4\Delta}$, CMV-Cre+;$Scyl1^{+/AIv4\Delta}$, $Scyl1^{-/AIv4\Delta}$, and $Scyl1^{-/AIv4}$mice were evaluated at 8 weeks of age. Growth abnormalities were measured by weighing the mice. Muscle strength was monitored by using an inverted cage grid test, as described previously (Pelletier et al., 2012). Additionally, motor dysfunction was assessed using a previously established scoring system where a score of 1 indicates visible growth abnormalities; 2 indicates growth defects and abnormal gait; 3 indicates posterior waddle and abnormal gait; 4 indicates growth abnormalities, abnormal gait, and tremor when suspended by their tails; 5 indicates aforementioned phenotypes and partial paralysis; 6 indicates complete paralysis; and 7 indicates flattening of the pelvis and dorsally contracted hindlimbs (Pelletier et al., 2012). For the grip test, mice were placed on top of an elevated cage grid. When mice were holding tightly to the cage grid, the grid was inverted and then the amount of time that they remained suspended (maximum 120 s) was recorded.

2.8. Histology

Histologic studies were performed on tissues collected from 3 females from each of the following genotypes: *Scyl1*$^{+/+}$, *Scyl1*$^{AIv4/AIv4}$, CMV-Cre+;*Scyl1*$^{AIv4\Delta/AIv4\Delta}$, and CMV-Cre+;*Scyl1*$^{+/AIv4\Delta}$. Immediately after the animals were sacrificed, right hindlimbs were postfixed by immersion in 4% paraformaldehyde in PBS for at least 24 h at 4 °C before being decalcified in formic acid. Tissues were embedded in paraffin, sectioned at 8 μm, mounted on positively charged glass slides, and dried in a 60 °C oven for 20 min. Slides were stained with hematoxylin and eosin (H&E) using LINISTAIN GLX linear stainer. Images of H&E-stained limb cross-sections were acquired with an Echo Revolve microscope.

2.9. RT-qPCR on brain tissues

Scyl1 expression was analyzed at the mRNA level using RT-qPCR. Briefly, cerebella were harvested from CMV-Cre+;*Scyl1*$^{AIv4\Delta/AIv4\Delta}$ and CMV-Cre+;*Scyl1*$^{+/+}$ mice, rinsed with PBS and snap frozen in liquid nitrogen. Total RNA was extracted using Rneasy Maxi Kit (Qiagen, 75162) with the RNase-Free DNase Set (Qiagen, 79254). The quality of the RNA was assessed using the Agilent TapeStation system and quantified by Nanodrop. cDNA was produced from 100 ng of total RNA using the ProtoScript® II First Strand cDNA Synthesis Kit (New England Biolabs, E6560L) with the d(T)$_{23}$ VN primer, according to the manufacturer's recommendations. *Scyl1 transcript* expression was quantified using TaqMan 2X Master Mix (Applied Biosystems, 4444557) and TaqMan Gene Expression Assay Probe Mm00452459_m1(FAM), which was normalized against *Gapdh* expression using TaqMan Gene Expression Assay Probe Mm99999915_g1 (FAM). Relative expression of *Scyl1* was determined using the ΔΔCt method.

2.10. RT-PCR

The detection of aberrant *Scyl1* transcripts was performed by RT-PCR using primers designed to amplify sequences between exon 2 to exon 5 (RT-Scyl1_F21 5′-CGCAGTGTCCATCTTCGTGTA-3′ and RT-Scyl1_R51 5′-CCCGGCAGTTCTGCAGGAA-3′) following the OneTaq One-Step RT-PCR Kit (New England Biolabs, E5315S) procedure. Briefly, cerebella were harvested from *Scyl1*$^{+/+}$, *Scyl1*$^{+/AIv4}$, *Scyl1*$^{AIv4/AIv4}$, CMV-Cre+;*Scyl1*$^{+/+}$, CMV-Cre+;*Scyl1*$^{+/AIv4}$, and CMV-Cre+;*Scyl1*$^{AIv4\Delta/AIv4\Delta}$ mice, rinsed with PBS and snap frozen in liquid nitrogen. Total RNA was extracted using Rneasy Maxi Kit (Qiagen, 75162) and the additional RNase-Free DNase digestion step (Qiagen, 79254). The quality and quantity of the RNA were assessed as described above.

2.11. SCYL1 isoform expression in SCYL1-KO Hek293T cells

For expression of SCYL1 isoforms produced from various transcript variants, mammalian expression plasmids encoding each variant were generated by removing specific sequences off a C-terminally tagged SCYL1 cDNA using QuikChange II XL Site-Directed Mutagenesis Kit (Agilent technologies, 200521). Each variant was transfected into SCYL1-KO Hek293T cells using Lipofectamine 2000 (ThermoFisher, 11668027) according to the manufacturer's recommendations, and their expression determined 48 h after transfection by western blotting using an anti-HA-Tag Antibody (F-7, sc-7392, Santa Cruz Biotechnology) as described in the "SCYL1 protein expression in mouse tissues" section. Band intensities were quantified by using NIH Image J software version 1.42q (http://rsbweb.nih.gov/ij) and normalized to β-actin. SCYL1 isoforms expression was further normalized to full length SCYL1. Because protein expression reflects not only translation and stability of the protein, but also the abundance of the transcript. SCYL1 isoform expression was also normalized to the amount of isoform transcript expressed in the cells. The amount of RNA transcript for each variant was determined by RT-qPCR as described above (from 2 independent experiments). Total RNA was extracted using the Rneasy Mini Kit (Qiagen, 74104).

2.12. SCYL1 isoform stability

Stability of SCYL1 and transcript variant isoforms was determined as described previously (Gingras et al., 2017). Briefly, SCYL1-KO Hek293T cells were transfected or not (Mock) with equal amounts of plasmids encoding HA-tagged SCYL1, or HA tagged versions of SCYL1 isoforms. 24 hours after transfection, cells were treated (or not) with cycloheximide (10 μg/mL) for 24, 6, 4 or 2 h. Proteins were extracted using Triton X-100 (Sigma-Aldrich, T8787-250ML) buffer supplemented with cOmplete™ and PhosSTOP™. 5 μg of total proteins were run on 10% Criterion™ XT Bis-Tris Protein Gels for separation, as described above. Protein expression was determined by western blotting using an anti-HA-Tag Antibody (F-7, sc-7392, Santa Cruz Biotechnology) as described in the "SCYL1 protein expression in mouse tissues" section.

2.13. Mouse husbandry

Mice were housed in an Association for Assessment and Accreditation of Laboratory Animal Care accredited facility and maintained in accordance with the National Institutes of Health Guide for the Care and Use of Laboratory Animals. Animal experiments were reviewed and approved by the Indiana University Institutional Animal Care and Use Committee.

3. Results

In search of more efficient and effective strategies to engineer conditional alleles in mice, we turned to a recently developed system called DECAI (Guzzardo et al., 2017). This approach consists of inserting a short 201-nucleotide-long DNA cassette within an exon of a gene. The cassette, here referred to as Artificial Intron version 4 (AIv4) as originally described in Guzzardo's manuscript, contains sequences encoding a splice donor, essential intronic sequences flanked by two loxP sites, and a splice acceptor (Figure 1A). In the absence of Cre, the intron is functional and removed by the splicing machinery, allowing for normal expression of the protein. In the presence of Cre, recombination between the two loxP sites occurs resulting in the removal of the branch point and part of the polypyrimidine tract. The crippled intron is then no longer recognized by the splicing machinery and remains within the transcript, leaving a string of stop codons in all three frames. This results in early translation termination and degradation of the damaged mRNA via the nonsense-mediated mRNA decay pathway.

To test whether this approach could be effectively used to engineer conditional alleles in mice, the cassette was inserted within exon 3 of the *Scyl1* gene via microinjection of pronuclear stage zygotes with Cas9 mRNA transcript, a single guide RNA (sgRNA), and a homology-directed repair (HDR) template in the form of a short single stranded DNA (ssDNA) molecule with sequences encoding the artificial intron flanked by homology arms of 58 and 60 nucleotides (Figure 1B). *Scyl1* was chosen as prototypic gene for two main reasons. First, *Scyl1* is an extensively studied gene in our laboratory and all the necessary reagents to characterize the mice are available to us, including highly specific antibodies, and mouse models bearing null and conditional alleles. Second, *Scyl1* deficiency results in dramatic and highly predictable phenotypes, including postnatal growth defects and an early onset motor neuron disorder reminiscent of amyotrophic lateral sclerosis (ALS), resulting in motor dysfunction and muscle wasting due to muscle denervation. Disease onset in *Scyl1*-deficient mice is 4 weeks of age. Full penetrance of the phenotypes can be seen by 12 weeks of age (Pelletier et al., 2012). From two rounds of microinjection, a total of 27 mice were obtained. 12 of these mice were edited by Cas9, and 2 contained the proper insertion (16.7% of edited mice). Sanger sequencing of TOPO cloned PCR fragments produced from primers external to the HDR template (S1E154D-F1 and S1E154D-R1, see method section for more details) confirmed the proper insertion of the artificial intron (Figure 1C).

One of the founder animals was then crossed to C57BL/6J mouse to generate F1 animals. All F1 mice taken forward were analyzed at the

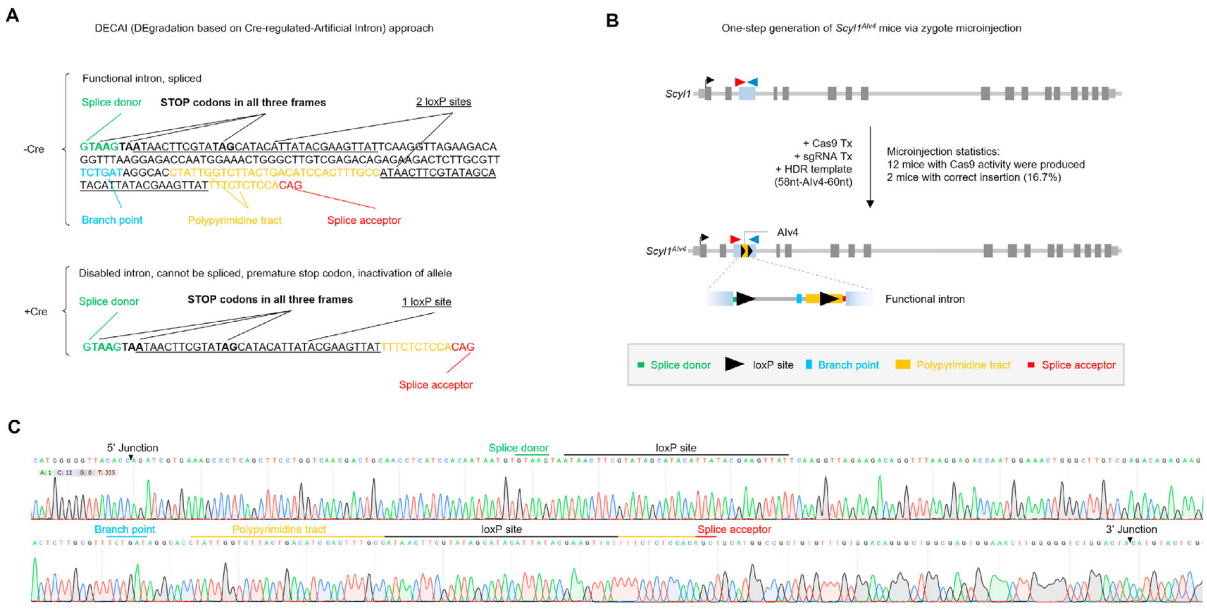

Figure 1. Generation of a *Scyl1* conditional allele in mice using the DECAI approach. A) The sequence for the artificial intron was derived from (Guzzardo et al., 2017), and contains sequences encoding a splice donor (green), followed by stop codons in all three frames (bold), a loxP site (underlined), a branch point (blue), a polypyrimidine tract (yellow), a second loxP site (underlined), and a splice acceptor (red). In the absence of Cre recombinase, the artificial intron is removed by the splicing machinery, allowing translation of the protein. Upon Cre-mediated recombination of the two loxP sites, the artificial intron is disabled such that after transcription and maturation of the transcript, the crippled intron cannot be removed, leading to early termination of translation and degradation of the mRNA transcript via the nonsense-mediated mRNA decay pathway. B) Schematic representation of the wild type *Scyl1* and $Scyl1^{AIv4}$ alleles and generation of $Scyl1^{AIv4}$ mice. Dark gray boxes represent exons, with exon 3 highlighted in blue. Light gray boxes represent the 5′ and 3′ untranslated regions of the gene. Red and blue triangles represent genotyping primers F51 and R52, respectively. The black arrowheads represent the start sites. The yellow box flanked by two black triangles represents the artificial intron inserted into exon 3 of *Scyl1*. $Scyl1^{AIv4}$ mice were engineered via pronuclear stage zygote microinjection with Cas9 mRNA transcript, a sgRNA targeting exon 3 of *Scyl1,* and an HDR template containing sequences encoding the artificial intron flanked by homology arms of 58 and 60 nucleotides. 12 mice with Cas9 activity were produced, 2 of which contained the artificial intron (16.7%). C) The sequence composition of the AIv4 allele was confirmed by TOPO-TA cloning and Sanger sequencing.

genomic level by PCR amplification, TOPO-TA cloning, and Sanger sequencing. Moreover, because random integrations of the donor template may occur in founder animals, all F1 mice produced from an outcross to C57BL/6 mice were also analyzed at the genomic level for evidence of random integrations. Given that the likelihood of having both a random integration and a targeted event in the same animal is extremely low (Lanza et al., 2018), random integration was evaluated in both $Scyl1^{AIv4}$-positive and $Scyl1^{AIv4}$-negative F1 animals. The presence of random integration(s) in $Scyl1^{AIv4}$-negative F1 animals would indicate that random integration(s) occurred. None of the $Scyl1^{AIv4}$-negative mice showed random integration, suggesting that only the targeted event occur in $Scyl1^{AIv4}$-positive mice, unless the event occurred on the same allele, which is unlikely (Figure 2A and 2B).

To test the functionality of the allele, F1 mice carrying the insertion were outbred to C57BL/6J mice and heterozygous mice produced from these outbreeds (F2) were used to generate wild-type ($Scyl1^{+/+}$), heterozygous ($Scyl1^{+/AIv4}$), and homozygous ($Scyl1^{AIv4/AIv4}$) mice. These mice were then analyzed at the genomic and protein levels by PCR amplification, Sanger sequencing, and western blotting using an antibody against SCYL1 that recognizes an epitope located within the carboxyl-terminal segment of SCYL1 (Figure 2C, 2D, 2E). Fragments of 304 base pairs (bp) corresponding to the wild-type allele were present in $Scyl1^{+/+}$ and $Scyl1^{+/AIv4}$ mice whereas fragments of 505 bp, corresponding to the allele containing the artificial intron, were observed in $Scyl1^{+/AIv4}$ and $Scyl1^{AIv4/AIv4}$ mice (Figure 2C). Sanger sequencing of PCR products obtained from both $Scyl1^{+/+}$ and $Scyl1^{AIv4/AIv4}$ mice confirmed the nature of the alleles. Importantly, SCYL1 protein expression was comparable in both $Scyl1^{+/+}$ and $Scyl1^{AIv4/AIv4}$ mice (Figure 2D and 2E), and $Scyl1^{AIv4/AIv4}$ mice showed no overt abnormalities, unlike *Scyl1*-deficient ($Scyl1^{-/-}$) mice (Pelletier et al., 2012), further supporting the view that the artificial intron is efficiently removed by the splicing machinery allowing for the proper expression of the protein.

To test whether recombination between the two loxP sites would occur despite their proximity (113 bp), $Scyl1^{AIv4/AIv4}$ mice were crossed with Cre-deleter mice which express Cre recombinase in virtually all tissues (B6.C-Tg (CMV-cre)1Cgn/J, abbreviated CMV-Cre+). From this cross, 33 mice were obtained, 16 of which expressed Cre and harbored a copy of the recombined AIv4 allele (AIv4Δ) (Figure 3A and 3B). Importantly, a recombination frequency greater than 80% was observed in Cre expressing mice (Figure 3C), suggesting that recombination occurred efficiently despite the proximity of the two loxP sites. As a comparison, the recombination frequency between 2 loxP sites flanking exons 2 to 17 of the *Scyl1* gene (~12.5 kb apart) was less than 50% (Figure 3A, 3D, and 3E). Mosaic deletion was also observed in several animals, which was likely the result of cellular mosaicism of Cre expression rather than the recombination inefficiency of the AIv4 cassette (Schwenk et al., 1995). Mosaic animals were not used for subsequent breeding.

To test whether recombination between the two loxP sites would result in the inactivation of *Scyl1*, CMV-Cre+;$Scyl1^{+/AIv4Δ}$ mice were crossed with $Scyl1^{AIv4/AIv4}$ mice to generate CMV-Cre+;$Scyl1^{AIv4Δ/AIv4Δ}$ mice. From this cross, 36 mice were obtained, 16 of which expressed Cre and 10 were also homozygous for the AIv4Δ allele (62.5% of Cre expressing mice) (Figure 4A and 4B). PCR fragments corresponding to the AIv4 and AIv4Δ alleles were analyzed by Sanger sequencing and confirmed the proper rearrangement of the recombined allele in Cre expressing mice (Figure 4C). Incomplete recombination was observed in some of these mice, which is consistent with the mosaic expression of Cre in CMV-Cre mice (Schwenk et al., 1995). These mice were excluded from subsequent analyses and crosses. Importantly, CMV-Cre+; $Scyl1^{AIv4Δ/AIv4Δ}$ mice, like $Scyl1^{-/-}$ mice, did not express SCYL1, as revealed by western blotting using an antibody against the

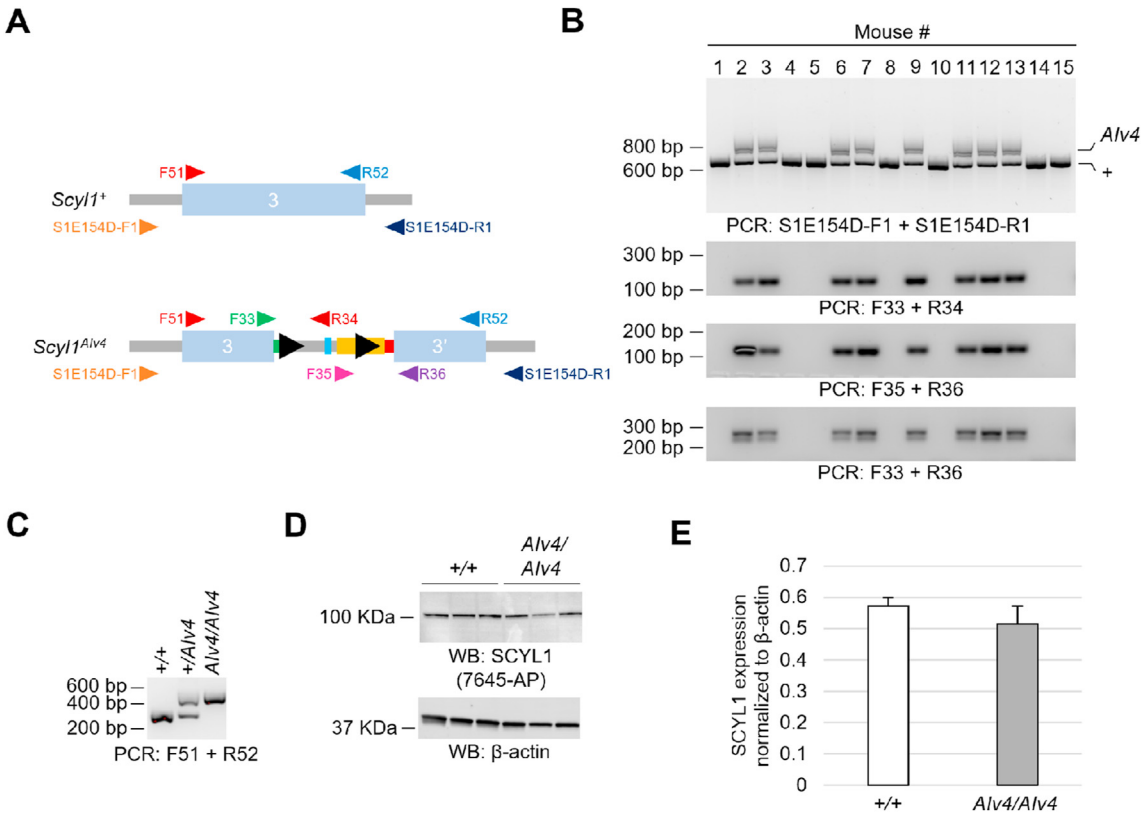

Figure 2. Functional validation of the *Scyl1*^{Aiv4} allele. A) Schematic representation of the modified exon 3 and primers used for the identification of *Scyl1*^{Aiv4} F1 animals and random integration of the cassette. B) On-target genotyping of F1 animals obtained from the founder animal used to establish the colony. PCR fragments were TOPO-TA cloned and sequenced to confirm the nature of the AIv4 allele. Random integration PCR using primer pairs F33 and R34, F35 and R36, and F33 and R36 are illustrated. Bands of 147 bp, 131 bp, and 280 bp were obtained, respectively. No random integrations were found in AIv4-negative animals suggesting that F1 animals do not contain randomly integrated HDR templates (see Methods and Results sections for details). C) PCR genotyping of *Scyl1*$^{+/+}$, *Scyl1*$^{+/Aiv4}$, and *Scyl1*$^{Aiv4/Aiv4}$ F3 animals obtained from F2 outbreeds. Amplicons of 304 bp correspond to the wild-type allele, whereas amplicons of 505 bp correspond to the AIv4 allele. D) SCYL1 expression in the brain of *Scyl1*$^{+/+}$ and *Scyl1*$^{Aiv4/Aiv4}$ mice, as detected by western blotting (top panel). β-actin Western blot (bottom panel) serves as loading control. E) Quantification of SCYL1 expression in the brain of *Scyl1*$^{+/+}$ and *Scyl1*$^{Aiv4/Aiv4}$ mice, normalized to β-actin. Data is expressed as mean ± SEM.

carboxyl-terminal segment of SCYL1 (7645-AP) (Figure 4D). Similarly, no expression of the full-length protein or shorter aberrant isoforms were observed in CMV-Cre+;*Scyl1*$^{AIv4\Delta/AIv4\Delta}$ mice when using an antibody against the amino-terminus of SCYL1 (Figure 4D). These results indicated that inactivation of the artificial intron via Cre-mediated recombination efficiently inactivated the allele and abrogated SCYL1 expression.

Previous studies in our laboratory have shown that inactivation of *Scyl1* results in growth retardation and severe motor dysfunction due to the progressive loss of spinal motor neurons (Kuliyev et al., 2018; Pelletier et al., 2012). To test whether inactivating the cassette would result in a loss-of-function phenotype, we monitored the weight, grip strength, and visually assessed motor dysfunction using a previously established scoring system (Kuliyev et al., 2018; Pelletier et al., 2012). Histology was also performed on the hindlimbs of these animals to look for signs of neurogenic atrophy. Consistent with complete inactivation of *Scyl1*, CMV-Cre+;*Scyl1*$^{AIv4\Delta/AIv4\Delta}$ mice exhibited growth retardation (Figure 5A and 5B), muscle weakness (Figure 5C) and muscle wasting (Figure 5C and 5E), as well as sensory motor deficits (Figure 5D). Muscle fibers in CMV-Cre+;*Scyl1*$^{AIv4\Delta/AIv4\Delta}$ mice showed evidence of neurogenic atrophy such as small angulated fibers, centrally localized nuclei, and group atrophy, similar to *Scyl1*-deficient mice (Figure 5F) (Kuliyev et al., 2018; Pelletier et al., 2012). To further demonstrate that the recombined *Scyl1*^{AIv4} allele results in complete inactivation, a complementation assay was performed by crossing *Scyl1*$^{+/AIv4}$ or *Scyl1*$^{+/AIv4\Delta}$ mice with *Scyl1*$^{+/-}$ mice. Consistent with the loss of function of the *Scyl1*$^{AIv4\Delta}$ allele, *Scyl1*$^{-/AIv4\Delta}$ mice did not express SCYL1 (Figure 6A) and exhibited growth retardation, muscle weakness and motor dysfunction (Figure 6B, 6C, 6D, 6E, 6F, 6G). Conversely, *Scyl1*$^{-/AIv4}$ mice expressed SCYL1 and showed no overt abnormalities (Figure 6A, 6B, 6C, 6D, 6E, 6F, 6G).

Although inactivation of the AIv4 cassette abrogated SCYL1 protein expression and resulted in phenotypic changes consistent with the loss of *Scyl1* function in vivo, *Scyl1* mRNA transcript levels remained essentially unchanged in *Scyl1*$^{AIv4\Delta/AIv4\Delta}$ mice compared to wild-type mice (Figure 7A). The presence of the transcript and the complete absence of SCYL1 protein suggested changes in the nature of the transcript expressed in *Scyl1*$^{AIv4\Delta/AIv4\Delta}$ mice. To test whether aberrant transcripts were produced from the *Scyl1*^{AIv4} or *Scyl1*$^{AIv4\Delta}$ alleles, a pair of primers was designed to amplify sequences spanning exons 2 to 5 of the *Scyl1* gene. RT-PCR reactions performed on total RNA samples from CMV-Cre+;*Scyl1*$^{+/AIv4\Delta}$ and CMV-Cre+;*Scyl1*$^{AIv4\Delta/AIv4\Delta}$ revealed the presence of shorter-than-predicted PCR fragments that likely corresponded to alternative splicing events (Figure 7B). These shorter PCR fragments were not observed in *Scyl1*$^{+/+}$, *Scyl1*$^{+/AIv4}$, *Scyl1*$^{AIv4/AIv4}$ or CMV-Cre+;*Scyl1*$^{+/+}$ mice, indicating that they likely resulted from the Cre-mediated recombination of the AIv4 cassette. TOPO-TA cloning and Sanger sequencing of the RT-PCR fragments revealed the presence of 5 distinct splice variants. Three of these variants were in frame. Of the two out-of-frame variants, one resulted from the predicted splicing event but accounted for only 4% of all transcripts present in the sample (transcript variant 4). The second out-of-frame variant, transcript variant 3, was also underrepresented and accounted for only 4% of all transcripts. The remaining three in-frame transcript variants accounted for nearly 92% of all transcripts present in the sample. These variants resulted from the splicing of the AIv4 splice donor site into the splice acceptor site of exon 4 (transcript variant 1), and accounted for the vast

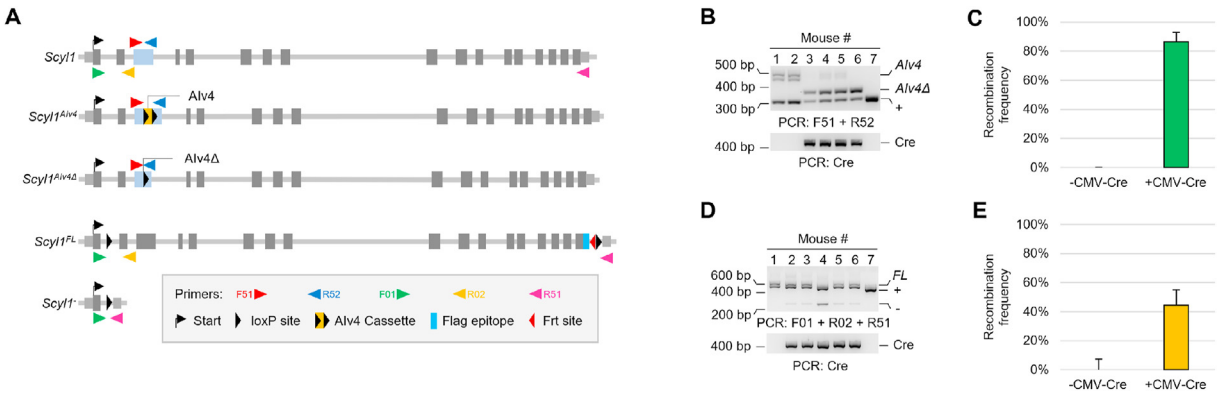

Figure 3. Recombination efficiency between the two loxP sites within the AIv4 cassette in vivo. A) Schematic representation of *Scyl1*$^{+}$, *Scyl1*^{AIv4}, *Scyl1*$^{AIv4\Delta}$, *Scyl1*^{FL}, and *Scyl1*$^{-}$ alleles. Dark gray boxes represent exons, with exon 3 highlighted in blue. Light gray boxes represent the 5′ and 3′ untranslated regions of the gene. Red, blue, green, yellow, and pink triangles represent genotyping primers F51, R52, F01, R02, and R51 respectively. The black arrowheads represent the start sites. The yellow box flanked by two black triangles (loxP sites) represents the artificial intron inserted into exon 3 of Scyl1. The light blue box represents a Flag epitope. The crimson triangle represents a Frt site. B) PCR based genotyping of mice obtained from CMV-Cre + mice crossed with *Scyl1*$^{AIv4/AIv4}$ mice. Amplicons of 304, 358, and 505 bp correspond to the wild-type, *Scyl1*$^{AIv4\Delta}$, and *Scyl1*^{AIv4} alleles, respectively. C) Quantification of recombination of the AIv4 allele into the AIv4Δ allele. Data is expressed as mean ± SEM. D) PCR based genotyping of CMV-Cre + mice crossed with *Scyl1*$^{FL/FL}$ mice. Amplicons of 521, 251, and 625 bp corresponding to the wild-type (*Scyl1*$^{+}$), null (*Scyl1*$^{-}$), and floxed alleles (*Scyl1*^{FL}), respectively, are obtained. E) Quantification of recombination of the floxed allele into the null allele. Data is expressed as mean ± SEM. Note the increased recombination efficiency in *Scyl1*$^{+/AIV4}$ mice compared to *Scyl1*$^{+/FL}$ mice.

majority of the in-frame variants (75%); the splicing of the AIv4 splice donor site into a cryptic splice acceptor site in exon 3, which accounted for 12.5% of all transcripts; and the splicing of a cryptic splice donor site in exon 3 into the AIv4 splice acceptor site, which accounted for 4.2% of all the transcripts (Figure 7C). The underrepresentation of the two out-of-frame variants, compared to in-frame variants, suggests that these transcripts may be degraded by the nonsense-mediated mRNA decay pathway, as predicted. The presence of in-frame transcripts also suggested that various protein isoforms may be produced from these transcripts. Western blot analyses, however, revealed the complete absence of SCYL1 in the brain of CMV-Cre+;*Scyl1*$^{AIv4\Delta/AIv4\Delta}$ animals (Figure 4D), suggesting that these mutant isoforms may be unstable and thus rapidly degraded after synthesis. To test this hypothesis, HA-tagged versions of transcript variants 1, 2, and 5 were ectopically expressed in *SCYL1*-deficient Hek293T cells (Gingras et al., 2017) and protein expression assessed by western blotting. As shown in Figure 7D and 7E, all three variants were expressed to much lower levels compared to the wild-type HA-tagged isoform. In fact, isoform 5 could not be detected (Figure 7D, 7E, 7F). From these results, we concluded that regulation of gene expression occurs not only at the transcriptional and translational levels but also at the post-translational level. Consistent with this, we found that the half-life of isoforms 1 and 2 were shortened compared to wild-type SCYL1 (Figure 7F). Acknowledging the existence of such in-frame splicing events is essential for proper design of additional alleles using this approach. Design considerations are presented in the discussion.

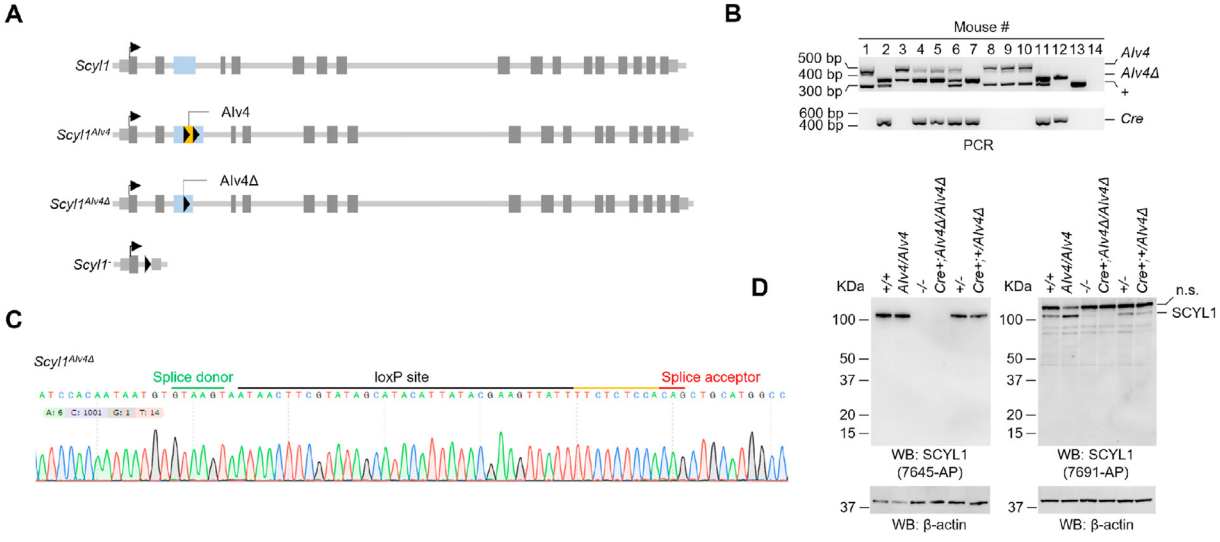

Figure 4. Cre-mediated disabling of the artificial intron leads to complete inactivation of *Scyl1*. A) Schematic representation of *Scyl1* alleles generated from this cross: *Scyl1*$^{+}$, *Scyl1*^{AIv4}, and *Scyl1*$^{AIv4\Delta}$. For comparison, *Scyl1*$^{-}$ is also illustrated. B) PCR-based genotyping of *Scyl1*$^{+}$, *Scyl1*^{AIv4}, and *Scyl1*$^{AIv4\Delta}$ alleles. Amplicons of 304, 358, and 505 bp correspond to the wild-type, *Scyl1*^{AIv4}, and *Scyl1*$^{AIv4\Delta}$ alleles, respectively. PCR primers for genotyping are illustrated in Figure 3A. C) Sanger sequencing was used to confirm proper recombination between the two loxP sites. D SCYL1 protein expression in the brain of *Scyl1*$^{+/+}$, *Scyl1*$^{AIv4/AIv4}$, *Scyl1*$^{-/-}$, CMV-Cre+;*Scyl1*$^{AIv4\Delta/AIv4\Delta}$, *Scyl1*$^{+/-}$, and CMV-Cre+;*Scyl1*$^{+/AIv4\Delta}$ mice, as detected by western blotting (top panel), using the anti-SCYL1 7645-AP antibody, which detects the C-terminal segment of SCYL1, or the anti-SCYL1 7691 antibody, which detects the N-terminus of the protein. Note the absence of SCYL1 proteins or any truncated isoforms in *Scyl1*$^{-/-}$, CMV-Cre+;*Scyl1*$^{AIv4\Delta/AIv4\Delta}$ mice. β-actin Western blot (bottom panel) serves as loading control.

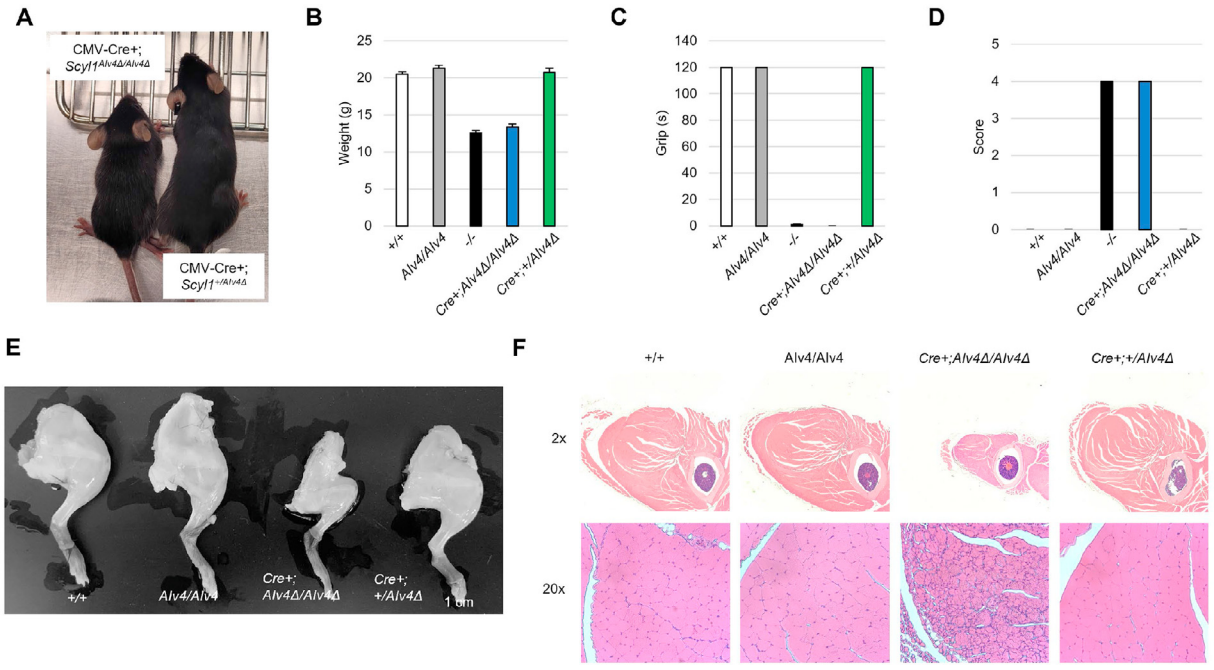

Figure 5. Complete inactivation of the AIv4 allele results in *Scyl1* loss-of-function phenotypes. A) Representative photograph of CMV-Cre+;$Scyl1^{AIv4\Delta/AIv4\Delta}$ and CMV-Cre+;$Scyl1^{+/AIv4\Delta}$ mice. Note the size difference between the littermates. B-D) Loss-of-function phenotypes in CMV-Cre+;$Scyl1^{AIv4\Delta/AIv4\Delta}$ mice. Similar to *Scyl1*-deficient mice, CMV-Cre+;$Scyl1^{AIv4\Delta/AIv4\Delta}$ mice exhibit growth retardation, sensory motor deficit, and muscle weakness. Data is expressed as mean ± SEM.
E) Representative photograph of the right hindlimbs of $Scyl1^{+/+}$, $Scyl1^{AIv4/AIv4}$, CMV-Cre+;$Scyl1^{AIv4\Delta/AIv4\Delta}$, and CMV-Cre+;$Scyl1^{+/AIv4\Delta}$ mice. F) Representative micrographs of H&E-stained sections of rectus femoris from 8-week-old $Scyl1^{+/+}$, $Scyl1^{AIv4/AIv4}$, CMV-Cre+;$Scyl1^{AIv4\Delta/AIv4\Delta}$, and CMV-Cre+;$Scyl1^{+/AIv4\Delta}$ mice. Note the presence of angulated/atrophied fibers in CMV-Cre+;$Scyl1^{AIv4\Delta/AIv4\Delta}$ mice.

4. Discussion

Here we describe the successful application of the DECAI approach for the generation of conditional alleles in mice via zygote injection of CRISPR-Cas9 components. The approach is straightforward, effective, and results in complete inactivation of the allele upon Cre-mediated recombination. The approach also provides several advantages over commonly used strategies and may represent a faster and more affordable solution to engineer conditional alleles in mice. Some modifications to the original strategy were also introduced to simplify the

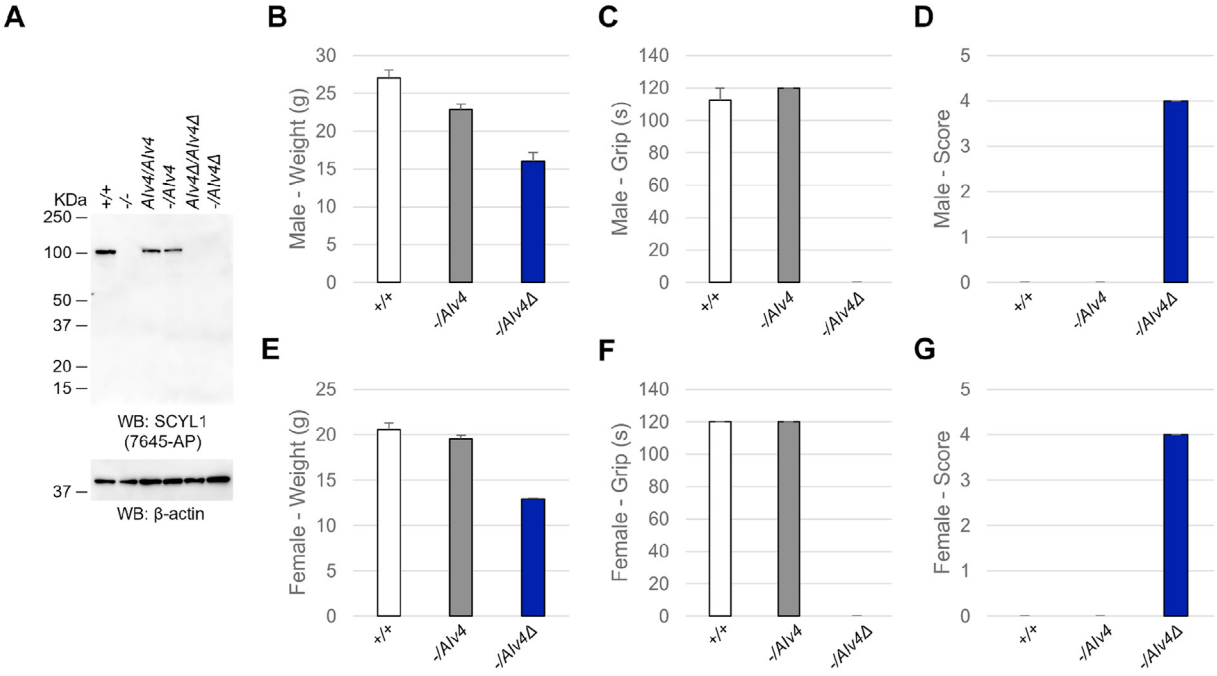

Figure 6. Complementation of the *Scyl1*$^{-}$ allele. A) SCYL1 expression in $Scyl1^{+/+}$, $Scyl1^{-/-}$, $Scyl1^{AIv4/AIv4}$, $Scyl1^{-/AIv4}$, $Scyl1^{AIv\Delta4/AIv\Delta4}$ and $Scyl1^{-/AIv4\Delta}$ mice. Note the lack of SCYL1 expression in $Scyl1^{-/-}$, $Scyl1^{AIv\Delta4/AIv4\Delta}$ and $Scyl1^{-/AIv4\Delta}$ mice. β-actin Western blot (bottom panel) serves as loading control.
B-G) Loss-of-function phenotypes in $Scyl1^{-/AIv4\Delta}$ but not $Scyl1^{-/AIv4}$ mice. Similar to *Scyl1*-deficient mice, but unlike $Scyl1^{-/AIv4}$, $Scyl1^{-/AIv4\Delta}$ mice exhibit growth retardation, sensory motor deficit, and muscle weakness. Data is expressed as mean ± SEM.

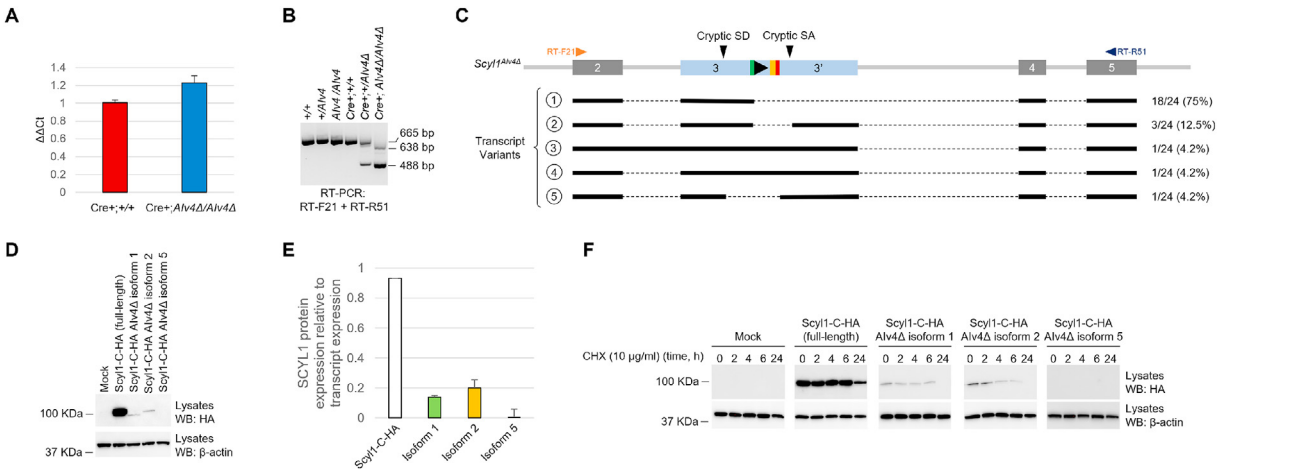

Figure 7. Transcript variants produced from the *Scyl1*$^{Alv4\Delta}$ allele. A) *Scyl1* transcript expression in the cerebella of CMV-Cre+;*Scyl1*$^{+/+}$ and CMV-Cre+;*Scyl1*$^{Alv4\Delta/Alv4\Delta}$ mice. Data is expressed as mean ± SEM. B) RT-PCR products generated from cerebellar total RNA extracts of *Scyl1*$^{+/+}$, *Scyl1*$^{+/Alv4}$, *Scyl1*$^{Alv4/Alv4}$, CMV-Cre+;*Scyl1*$^{+/+}$, CMV-Cre+;*Scyl1*$^{+/Alv4\Delta}$, and CMV-Cre+;*Scyl1*$^{Alv4\Delta/Alv4\Delta}$ mice. Amplicons of 665, 638, and 488 bp, corresponding to the mature form of the *Scyl1* transcript, as well as shorter transcript variants 1 and 2 were obtained. These shorter transcripts were observed only in CMV-Cre+;*Scyl1*$^{+/Alv4\Delta}$ and CMV-Cre+;*Scyl1*$^{Alv4\Delta/Alv4\Delta}$ mice. C) Schematic representation of the five most abundant RNA transcripts observed in CMV-Cre+;*Scyl1*$^{Alv4\Delta/Alv4\Delta}$ mice (transcripts variants labeled 1–5). RT-PCR products from CMV-Cre+;*Scyl1*$^{Alv4\Delta/Alv4\Delta}$ mice were TOPO cloned. Plasmid DNA was recovered from 24 clones and analyzed by Sanger sequencing. The frequency of each transcript is illustrated to the right of the transcript. 18 out of 24 clones were obtained for transcript variant 1; 3 out of 24 clones were obtained for transcript variant 2; and 1 out of 24 clones were obtained for transcript variants 3, 4, and 5. Transcript variant 1 resulted from the splicing of the AIv4 splice donor site into the splice acceptor site of exon 4. Transcript variant 2 resulted from the splicing of the AIv4 splice donor site into a cryptic splice acceptor site within the 3′ half of exon 3. Transcript variant 3 contained intronic sequences from intron 2 and the recombined AIv4 cassette as well as sequences encoding exon 2 to 5. Transcript variant 4 contained the expected sequence of the recombined AIv4 cassette. Transcript variant 5 resulted from the splicing of a cryptic splice donor site within the 5′ half of exon 3 into the AIv4 splice acceptor site. D) Ectopic expression of HA tagged versions of wild type, transcript variant 1, 2 and 5 under the control of the CMV promoter. All three isoforms generated from transcript variants 1, 2 and 5 were expressed at a much lower level than their wild-type, full length, counterpart. The images are representative of 3 independent experiments. E) Quantification of SCYL1 isoforms expression normalized to transcript variant expression. F) Stability of SCYL1 isoforms. SCYL1-KO Hek293T cells were transfected, or not (Mock) with equal amounts of plasmids encoding the HA-tagged version of full length SCYL1, transcript variant 1, 2 or 5. 24 hours after transfection, Cells were treated or not (0 h time point) with 10 μg/mL cycloheximide (CHX) for 24, 6, 4, and 2 h. SCYL1 protein expression was evaluated by western blotting using the anti-SCYL1 antibody 7645-AP. The images are representative of 2 independent experiments.

engineering process and improve efficiency. Finally, considering our findings, we provide guidelines for the design of alleles using this approach.

Currently, there are two main strategies employed to engineer conditional alleles in mice: the flanking of one or more critical exons with SSRSs or the insertion of large modules within an exon of a gene. Both design strategies can be used to engineer conditional alleles in mice via conventional or CRISPR-assisted gene targeting in ES cells or via microinjection of CRISPR components directly into pronuclear stage zygotes. While these approaches have been used to engineer several thousands of mouse models over the past decades, these approaches are labor intensive and inefficient. Flanking critical exons using conventional or CRISPR-assisted gene targeting in ES cells involves the generation of large targeting constructs and often requires screening of several hundred clones. These approaches also often involve selection markers, leaving genetic scars at the engineered loci. Moreover, several rounds blastocyst injections are often needed to obtain chimeric animals capable of transmitting the genetic alteration. Flanking exons with SSRSs via zygote microinjection of CRISPR reagents and short ssDNA molecules encoding SSRSs flanked by short homology arms also has its share of limitations. SSRSs must be inserted in cis which significantly reduces the chance of generating floxed alleles (Pelletier et al., 2015). Although the use of large DNA molecules encoding both SSRSs were shown to improve this process (Codner et al., 2018; Miura et al., 2018; Quadros et al., 2017), their synthesis is expensive, frequently unsuccessful, and the molecules are often too small to flank multiple exons. Additionally, the approach of flanking exons with SSRSs cannot be used to inactivate single exon or overlapping genes, as the insertion of SSRSs may disrupt regulatory elements within the promoter or the 3' UTR of those genes. The use of large artificial introns for engineering conditional alleles in mice also share many of the aforementioned constraints, as these are typically used for gene targeting in ES cells and require the generation of large, complex targeting constructs (Andersson-Rolf et al., 2017; Economides et al., 2013). Moreover, these rely on the activity of a splice acceptor site which can be leaky, allowing for expression of the target gene, as well as strong promoters within reporter cassettes, which may affect the expression of surrounding genes (Andersson-Rolf et al., 2017; Economides et al., 2013; Soulez et al., 2019).

The modified DECAI approach described here makes use of a short 319-nucleotide-long ssDNA molecule as an HDR template to insert a 201-nucleotide-long cassette. Short ssDNA molecules are inexpensive, generally easy to synthesize, and are efficiently inserted via microinjection of CRIPSR reagents into pronuclear stage zygotes (Pelletier et al., 2015), bypassing the need to engineer ES cells. Insertion of the small artificial intron used in our study occurred in 16.7% of edited pups obtained from zygote injection. More recently, we obtained insertional rates of 50%, 100% and 60% for three other models. These results suggest that a single round of injection may be sufficient to generate conditional alleles in mice using this methodology. The genotyping of such an allele is also greatly simplified compared to genotyping floxed alleles or conditional alleles generated using large molecules as it only requires a single pair of primers, PCR amplification of the locus, and Sanger sequencing. Another foreseeable advantage of using this technology to engineer conditional alleles in mice is that, like most CRISPR-based approaches, it can be multiplexed and several alleles can be engineered from a single round of microinjection. Alleles can be subsequently segregated by outbreeding founder mice with wild type animals. This approach is currently being tested in our facility. If successful, multiplexing may again significantly reduce the cost and time required for engineering conditional alleles in mice. Although not tested here, the approach can also be used to conditionally inactivate single exon genes as well as overlapping genes as the modification affects gene expression at the mRNA and/or translational level rather than at the structural level of the gene.

Despite the numerous advantages of this approach, some potential limitations to the use of this technology may exist. For example, the preference of GT-AG introns for specific sequences upstream and downstream of the splice donor and acceptor sites may limit the number of possible target sites for insertion of the intron (Sibley et al., 2016). These sequences generally contain a CAG or AAG upstream of the donor site and an A or G immediately downstream of the splice acceptor site. However, when engineering the *Scyl1*^{AIv4} allele, this notion was overlooked and the artificial intron was inserted two nucleotides upstream of the SpCas9 cut site, immediately after a TGT and before a C. While these sequences are thought to be suboptimal to promote splicing (Sibley et al., 2016), SCYL1 expression in *Scyl1*$^{AIv4/AIv4}$ and *Scyl1*$^{+/+}$ mice was similar, indicating that the artificial intron is efficiently removed by the splicing machinery. Thus, limiting the insertion of the AIv4 cassette to CAG-A/G or AAG-A/G sites may not be required for engineering conditional alleles using this approach.

Another potential downside of using this technology is that insertion of the intron may affect gene expression by deregulating endogenous splicing events (Guzzardo et al., 2017). Although RT-PCR and western blotting results presented here indicate that no such dysregulation occurred in *Scyl1*$^{AIv4/AIv4}$ mice, aberrant splicing events in CMV-Cre+;*Scyl1*$^{+/AIv4\Delta}$ and CMV-Cre+;*Scyl1*$^{AIv4\Delta/AIv4\Delta}$ mice were observed. These aberrant splicing events were only observed when the AIv4 polypyrimidine tract and the branch point were removed via Cre-mediated recombination, indicating that crippling of the intron leaves behind an active splice donor site that drives unpredictable and potentially undesirable splicing events. This observation is extremely important and should not be disregarded, especially if these splicing events are in-frame, as mutant forms of the protein with aberrant properties may be expressed. Fortunately, no mutant forms of SCYL1 were detected by western blotting using antibodies against the amino-terminal or the carboxyl-terminal segment of SCYL1, suggesting that if truncated forms of SCYL1 were produced, they were likely unstable and immediately degraded after synthesis. Consistent with the generation of a loss-of-function allele, CMV-Cre+;*Scyl1*$^{AIv4\Delta/AIv4\Delta}$ also exhibited growth retardation and motor dysfunction.

Two main splicing events were identified in CMV-Cre+;*Scyl1*$^{AIv4\Delta/AIv4\Delta}$ mice. The first was a splicing event between the splice donor of AIv4 and the splice acceptor of exon 4 (transcript variant 1), which accounted for 75% of the transcripts. The second was the splicing between the AIv4 splice donor and a cryptic splice acceptor site located within the 3' half of exon 3 (transcript variant 2), which accounted for 12.5% of all transcripts. Both splicing events resulted in in-frame and thus functional transcripts which could have resulted in the expression of SCYL1 isoforms with aberrant properties. Although this was not the case, we suspect that the vast majority of the RNA transcript detected by RT-qPCR were either transcript variant 1 or 2. The low representation of the out-of-frame variants, including the expected transcript containing the recombined AIv4 allele (transcript variant 4), may result from their degradation via the nonsense-mediated mRNA decay pathway. In light of these findings, we propose the following guidelines for the generation of conditional alleles using AIv4.

1) The cassette should be inserted within the 5′ most exons of a gene and within the 5′ half of an exon to promote mRNA degradation via the nonsense-mediated mRNA decay pathway (Popp and Maquat, 2016).
2) The artificial intron should be inserted such that potential splicing events driven by the AIv4 splice donor with downstream exon(s) results in out-of-frame transcripts.
3) The placement of the artificial intron should not be limited by the availability of optimal sequences upstream of the splice donor and downstream of splice acceptor sites.

In conclusion, we believe that the application of this technology may significantly reduce the cost and time required for making mouse models with conditional alleles. Design considerations such as those presented herein are essential to the successful application of this technology.

Declarations

Author contribution statement

Stephane Pelletier, Ph.D.: Conceived and designed the experiments; Performed the experiments; Analyzed and interpreted the data; Contributed reagents, materials, analysis tools or data; Wrote the paper.

Annelise M Cassidy: Conceived and designed the experiments; Performed the experiments; Analyzed and interpreted the data; Wrote the paper.

Destinée B Thomas; Hanying Chen: Performed the experiments.

Emin Kuliyev: Performed the experiments; Analyzed and interpreted the data.

Funding statement

This work was supported by the Indiana University School of Medicine and the Department of Medical and Molecular Genetics.

Data availability statement

Data included in article/supp. material/referenced in article.

Declaration of interest's statement

The authors declare no conflict of interest.

Additional information

Supplementary content related to this article has been published online at https://doi.org/10.1016/j.heliyon.2022.e12630.

Acknowledgements

The authors would like to thank members of the Indiana University Genome Editing Center (IUGEC) for rederiving the *Scyl1*^{AIv4} mouse model, the St. Jude children's Research Hospital Transgenic and knockout core facility for microinjections, and the Histology Core of the Indiana Center for Musculoskeletal Health at IU School of Medicine and the Bone and Body Composition Core of the Indiana Clinical Translational Sciences Institute (CTSI) for skeletal muscle histology. Funding supporting this work was provided by the Indiana University School of Medicine and the Department of Medical and Molecular Genetics.

References

Andersson-Rolf, A., Mustata, R.C., Merenda, A., Kim, J., Perera, S., Grego, T., Andrews, K., Tremble, K., Silva, J.C., Fink, J., et al., 2017. One-step generation of conditional and reversible gene knockouts. Nat. Methods 14, 287–289.

Cassidy, A.M., Kuliyev, E., Thomas, D.B., Chen, H., Pelletier, S., 2022. Dissecting protein function in vivo: engineering allelic series in mice using CRISPR-Cas9 technology. Methods Enzymol. 667, 775–812.

Codner, G.F., Mianne, J., Caulder, A., Loeffler, J., Fell, R., King, R., Allan, A.J., Mackenzie, M., Pike, F.J., McCabe, C.V., et al., 2018. Application of long single-stranded DNA donors in genome editing: generation and validation of mouse mutants. BMC Biol. 16, 70.

Economides, A.N., Frendewey, D., Yang, P., Dominguez, M.G., Dore, A.T., Lobov, I.B., Persaud, T., Rojas, J., McClain, J., Lengyel, P., et al., 2013. Conditionals by inversion provide a universal method for the generation of conditional alleles. Proc. Natl. Acad. Sci. U. S. A. 110, E3179–3188.

Gingras, S., Kuliyev, E., Pelletier, S., 2017. SCYL1 does not regulate REST expression and turnover. PLoS One 12, e0178680.

Guzzardo, P.M., Rashkova, C., Dos Santos, R.L., Tehrani, R., Collin, P., Burckstummer, T., 2017. A small cassette enables conditional gene inactivation by CRISPR/Cas9. Sci. Rep. 7, 16770.

Kuliyev, E., Gingras, S., Guy, C.S., Howell, S., Vogel, P., Pelletier, S., 2018. Overlapping role of SCYL1 and SCYL3 in maintaining motor neuron viability. J. Neurosci. 38, 2615–2630.

Lanza, D.G., Gaspero, A., Lorenzo, I., Liao, L., Zheng, P., Wang, Y., Deng, Y., Cheng, C., Zhang, C., Seavitt, J.R., et al., 2018. Comparative analysis of single-stranded DNA donors to generate conditional null mouse alleles. BMC Biol. 16, 69.

Miura, H., Quadros, R.M., Gurumurthy, C.B., Ohtsuka, M., 2018. Easi-CRISPR for creating knock-in and conditional knockout mouse models using long ssDNA donors. Nat. Protoc. 13, 195–215.

Pelletier, S., Gingras, S., Green, D.R., 2015. Mouse genome engineering via CRISPR-Cas9 for study of immune function. Immunity 42, 18–27.

Pelletier, S., Gingras, S., Howell, S., Vogel, P., Ihle, J.N., 2012. An early onset progressive motor neuron disorder in Scyl1-deficient mice is associated with mislocalization of TDP-43. J. Neurosci. 32, 16560–16573.

Popp, M.W., Maquat, L.E., 2016. Leveraging rules of nonsense-mediated mRNA decay for genome engineering and personalized medicine. Cell 165, 1319–1322.

Quadros, R.M., Miura, H., Harms, D.W., Akatsuka, H., Sato, T., Aida, T., Redder, R., Richardson, G.P., Inagaki, Y., Sakai, D., et al., 2017. Easi-CRISPR: a robust method for one-step generation of mice carrying conditional and insertion alleles using long ssDNA donors and CRISPR ribonucleoproteins. Genome Biol. 18, 92.

Schwenk, F., Baron, U., Rajewsky, K., 1995. A cre-transgenic mouse strain for the ubiquitous deletion of loxP-flanked gene segments including deletion in germ cells. Nucleic Acids Res. 23, 5080–5081.

Sibley, C.R., Blazquez, L., Ule, J., 2016. Lessons from non-canonical splicing. Nat. Rev. Genet. 17, 407–421.

Soulez, M., Saba-El-Leil, M.K., Turgeon, B., Mathien, S., Coulombe, P., Klinger, S., Rousseau, J., Levesque, K., Meloche, S., 2019. Reevaluation of the role of extracellular signal-regulated kinase 3 in perinatal survival and postnatal growth using new genetically engineered mouse models. Mol. Cell Biol. 39.